

On the Sensitivity of Wall Stresses in Diseased Arteries to Variable Material Properties

S. D. Williamson, Y. Lam, H. F. Younis,
H. Huang, S. Patel, M. R. Kaazempur-Mofrad,
and R. D. Kamm

Department of Mechanical Engineering and the Biological Engineering Division, Massachusetts Institute of Technology, Cambridge, MA 02139

Accurate estimates of stress in an atherosclerotic lesion require knowledge of the material properties of its components (e.g., normal wall, fibrous plaque, calcified regions, lipid pools) that can only be approximated. This leads to considerable uncertainty in these computational predictions. A study was conducted to test the sensitivity of predicted levels of stress and strain to the parameter values of plaque used in finite element analysis. Results show that the stresses within the arterial wall, fibrous plaque, calcified plaque, and lipid pool have low sensitivities for variation in the elastic modulus. Even a $\pm 50\%$ variation in elastic modulus leads to less than a 10% change in stress at the site of rupture. Sensitivity to variations in elastic modulus is comparable between isotropic nonlinear, isotropic nonlinear with residual strains, and transversely isotropic linear models. Therefore, stress analysis may be used with confidence that uncertainty in the material properties generates relatively small errors in the prediction of wall stresses. Either isotropic nonlinear or anisotropic linear models provide useful estimates, however the predictions in regions of stress concentration (e.g., the site of rupture) are somewhat more sensitive to the specific model used, increasing by up to 30% from the isotropic nonlinear to orthotropic model in the present example. Changes resulting from the introduction of residual stresses are much smaller. [DOI: 10.1115/1.1537736]

Keywords: Atherosclerosis, Stress Analysis, Finite Element Analysis, Plaque Rupture

Introduction

Although the precise mechanisms of plaque rupture are not yet fully understood, structural analyses of arteries suggest that rupture occurs in areas of high stress concentration [1,2]. In that the

stress concentrations are critically dependent upon the geometry and mechanical properties of the lesion, the potential exists for using computational analysis of the stress distribution in conjunction with magnetic resonance or ultrasound imaging as a diagnostic tool. Accurate estimates of stress, however, require knowledge of the material properties of the different regions within the wall (e.g., normal wall, fibrous plaque, calcified regions, lipid pools) that can only be approximated and have been shown to be widely variable [3,4,8]. Thus there is considerable potential uncertainty in these computational predictions.

The purpose of this study is to test the sensitivity of predicted levels of stress to these material properties. Strains are also considered since wall deformation has been implicated in the stimulation of secretion, synthesis and gene expression in connection with a variety of factors implicated in the disease process. Models for analysis include isotropic nonlinear and anisotropic linear. Residual strains were also incorporated into the isotropic nonlinear model for further analysis.

Methods

Overview. Finite element analysis was applied to a typical two-dimensional cross-section of a diseased, ruptured artery excised post mortem. In order to generate the pre-ruptured geometry, we examined a post mortem specimen obtained from the coronary artery (Fig. 1). Regions of artery wall, fibrous plaque, lipid deposits, and calcified plaque were identified in a histological cross-section of the specimen. An investigator not involved in the current study reconstructed the pre-rupture, *in vivo* geometry, from which a model was generated using the commercial package OPTIMAS (Media Cybernetics, Silver Spring, MD). This geometry and its imposed boundary conditions were then used to create a finite element model.

Parameters. Fibrous plaque and arterial wall are each initially modeled as linearly elastic, orthotropic materials due to the in-plane load carrying capability of their collagenous components. Their mechanical properties are described by E_r and E_θ (Young's moduli in the r and θ directions, respectively), $\nu_{r\theta}$ and $\nu_{\theta z}$ (Poisson's ratios in the r - θ and θ - z planes, respectively), and $G_{r\theta}$ (shear modulus in the r - θ plane) [1,6]. The properties in the θ -direction are taken to be the same as for the z -direction, constituting a transversely isotropic material.

In determining the anisotropic parameters, E_θ for the plaque and artery were taken from the most recent data known at the time of this study [4]. In the same reference, E_r was estimated to be 5% of E_θ . The value of $\nu_{\theta z}$ is based on previous data from canine aortas [5]. From these numbers, $\nu_{r\theta}$ was then calculated to satisfy the conditions for a positive-definitive stiffness matrix [6]. The value for $G_{r\theta}$ was calculated as the average of its upper and lower limits, the upper bound taken as E_θ , the lower bound calculated by modeling the materials as incompressible and isotropic, in which case, $G_{r\theta} = (E_r/3)$ [7]. Therefore, the resulting value of $G_{r\theta} = [E_\theta + (E_r/3)]/2$ was used.

Calcified plaque and lipid are assumed to be linearly elastic, (nearly) incompressible, isotropic materials. Their mechanical

Corresponding Author: Roger D. Kamm, 77 Massachusetts Avenue, Room 3-260, Cambridge, MA 02139 Phone: (617) 253-5330; Fax: (617) 258-8559; E-mail: rdkamm@mit.edu

Contributed by the Bioengineering Division for publication in the JOURNAL OF BIOMECHANICAL ENGINEERING. Manuscript received June 2000; revised manuscript received July 2002. Associate Editor: J. D. Humphrey.

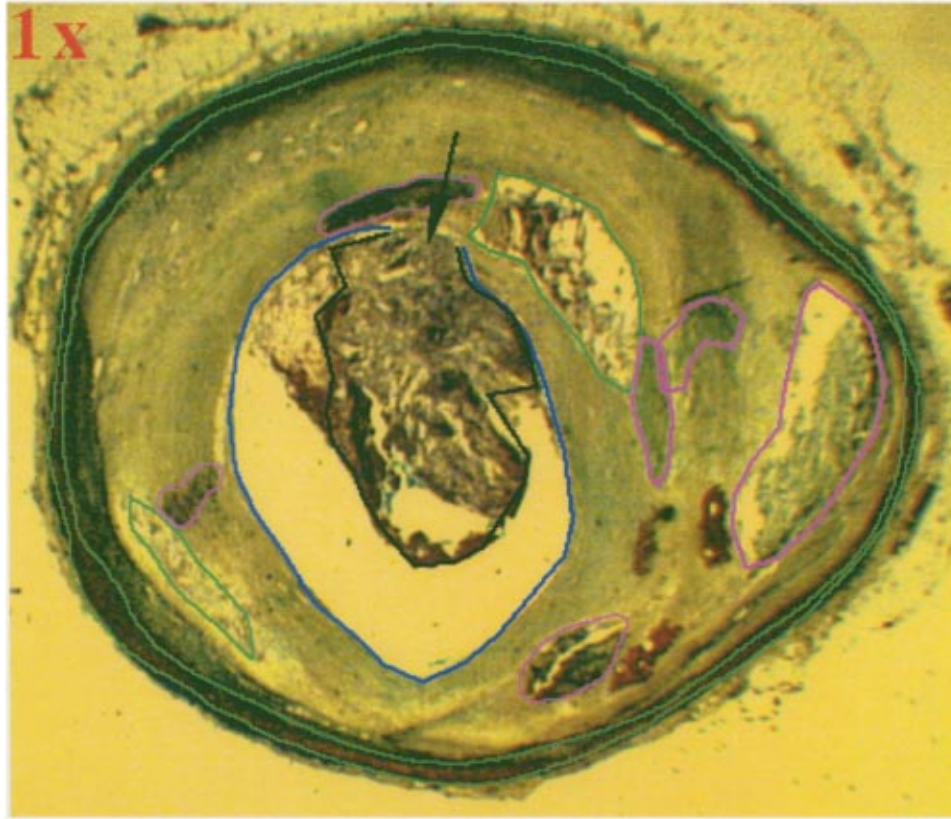


Fig. 1 Histology of the post mortem specimen obtained from the coronary artery. Segmentation provided by Dr. Renu Virmani.

properties are described by E , the Young's modulus and ν , Poisson's ratio. Values for E were taken from recent measurements [4,8], and a value of 0.45 was chosen for ν , slightly smaller than that for an incompressible material to avoid complications in the solution procedure. The resulting parameters are summarized in Table 1.

In order to incorporate non-linear behavior, the specimen was also modeled using the standard Lagrangian formulation for large displacements and large strains [9]. An isotropic form of the strain energy density function (SEDF) for the (nearly) incompressible artery wall is specified [10]:

$$W = \frac{a}{b} \left(e^{b/2(I_1 - 3)} - 1 \right) \quad (1)$$

where a and b are constants (Table 2) that reflect the elastic prop-

Table 1 Anisotropic linear material parameters.

	ARTERY	FIBROUS	CALCIFIED	LIPID
E_r (kPa)	10.0	115.6		
E_θ (kPa)	100.0	2312.0	1466	0.345
$\nu_{r\theta}$	1.00	1.35		
$\nu_{\theta z}$	0.27	0.27	0.45	0.45
$G_{r\theta}$ (kPa)	51.67	1175.27		

Table 2 Isotropic non-linear material parameters.

Material	a (kPa)	b
Artery	33.333	16.73
Fibrous Plaque	770.667	40.0
Calcified Plaque	488.667	30.0
Lipid	0.115	5.0

erties and tissue composition; I_1 is the first invariant of the strain tensor. In the Taylor series expansion, a has the significance of the elastic modulus; b is related to the strain-stiffening behavior of the material. The data of Loree et al. [8] were used to obtain the values a and b by matching to the average of the uniaxial stress-strain curves in the θ direction. This SEDF, despite being isotropic, has been shown to perform well as compared to other forms found in the literature [11]. Its predicted response is in good qualitative agreement with experimental measurements since it describes the well-known strain stiffening behavior of arteries.

Finite Element Analysis. The finite element analysis was carried out using ADINA, version 7.3 for the anisotropic case, version 7.4 for the isotropic nonlinear case, and version 7.5 for the isotropic nonlinear case with residual strain [12]. Using the geometry created from the histology specimen, a computational mesh was generated with quadrilateral, nine-node, plane-strain elements (Fig. 2). These elements have a local dimension of 0.03 mm, thereby allowing for accuracy particularly near material interfaces [1]. Mesh refinement by doubling the number of elements in the vicinity of the rupture point produced results that were generally within 0.4% of those from the original mesh. For the anisotropic model, displacement-based elements were used and for the isotropic models, displacement/pressure (u/p) based elements were used to avoid locking as ν approached 0.5 [9].

Residual strains were applied to the isotropic nonlinear model in order to produce a model with smaller radial stress gradients at normal arterial pressure, as typically found in normal, healthy arteries [3,10]. Strain values from the inflated isotropic model were averaged over 15 degree segments. This average value per segment was then subtracted from each of the original (inflated) strain values in that segment, node by node (done repetitively for each of the 15 degree segments). These differences were then applied to the model as nodal initial strains (Fig. 3).

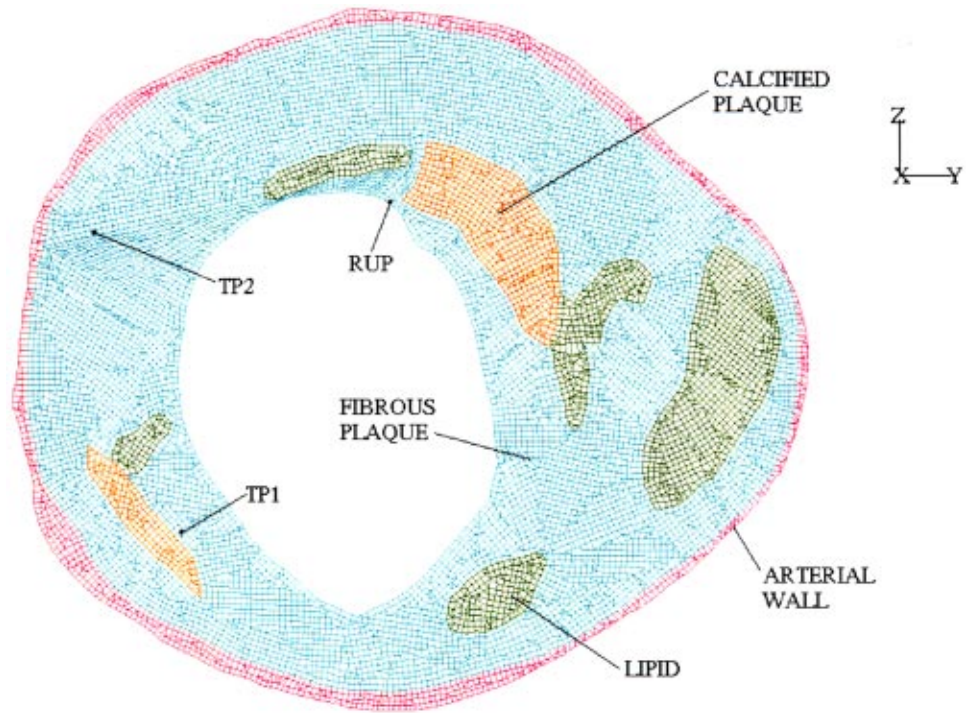


Fig. 2 Computational mesh with the model test points labeled. Red indicates normal arterial wall (media and adventitia combined), blue, fibrous plaque, purple, calcified plaque, and green, lipid pools.

Orthotropic axes were defined for each element, roughly corresponding to the circumferential and radial directions. Once the model was defined, the load was then ramped to an intraluminal static pressure of 14.6 kPa (110 mmHg); external pressure was assumed to be zero. The resulting mesh contained 44,450 nodes, 11,554 elements, and 110 surfaces. Maximum principal stress and maximum principal strain are determined at three points of inter-

est: (1) an element between a lipid pool and the lumen, denoted as Test Point 1 (TP1), (2) an element where the plaque is relatively homogeneous, denoted as Test Point 2 (TP2), and (3) the node, denoted as RUP, where plaque rupture occurred *in vivo* (Fig. 2).

Sensitivity Analysis. To observe the sensitivity of these material parameters, the models were first analyzed at the baseline

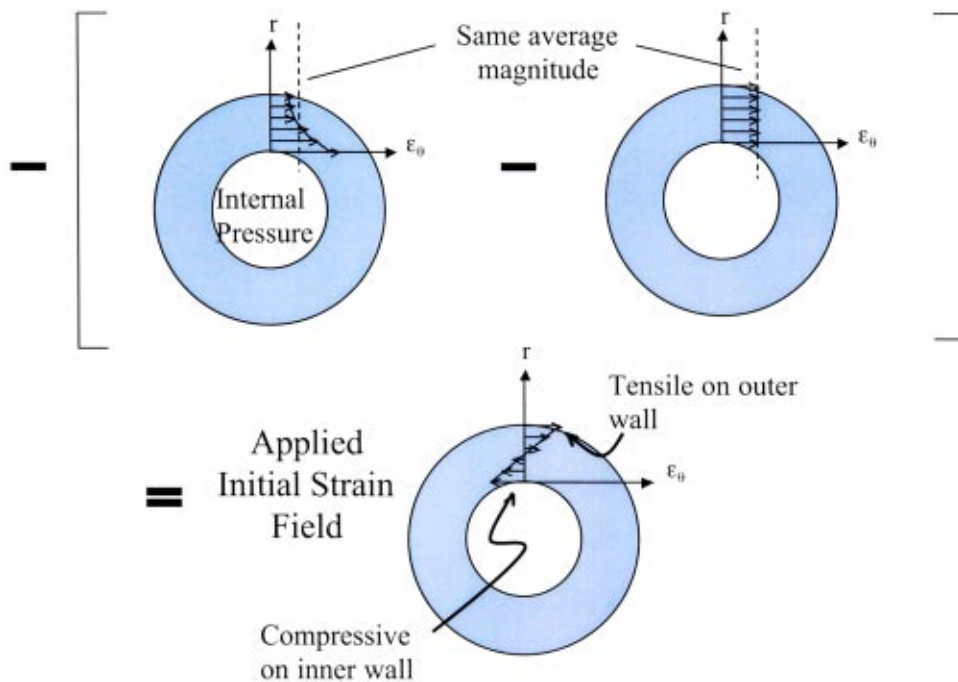
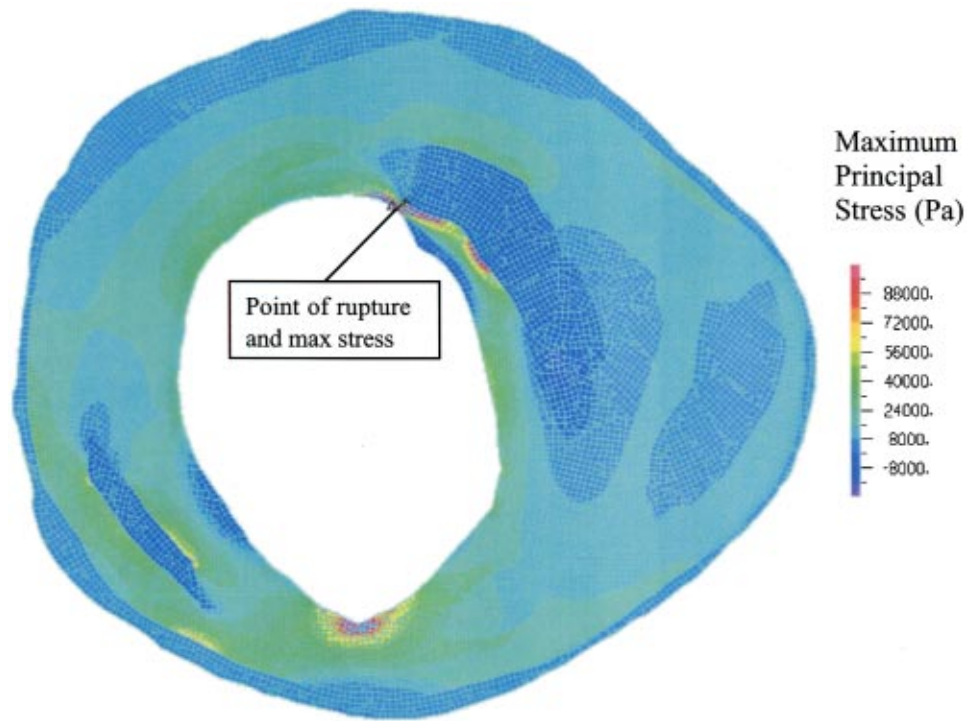
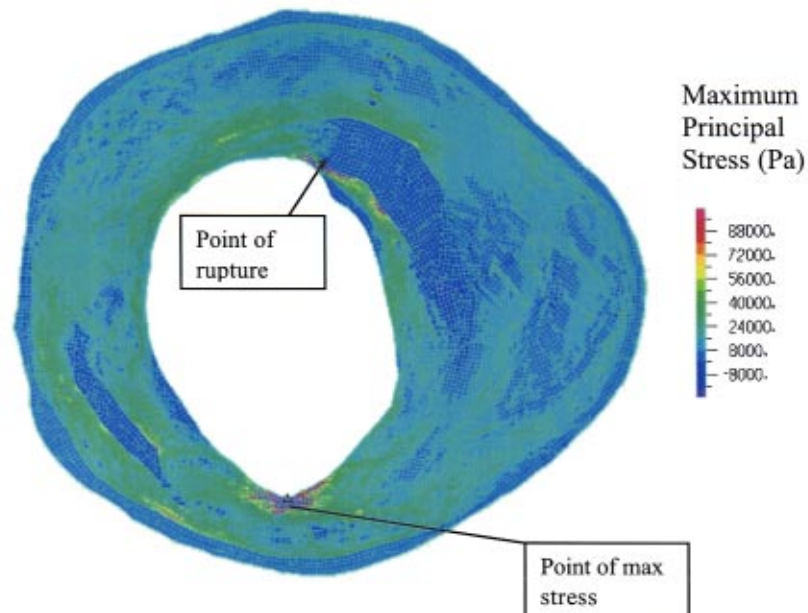


Fig. 3 Diagram of residual stress calculation and application.



(a)



(b)

Fig. 4 Maximum principal stress band plot (in Pa) for isotropic trials using average parameters. The triangle indicates the location of maximum stress while the star indicates the location of minimum stress. Nonlinear isotropic (a) and nonlinear isotropic with residual stresses (b). In the nonlinear isotropic run, the location of maximum stress is also the rupture site.

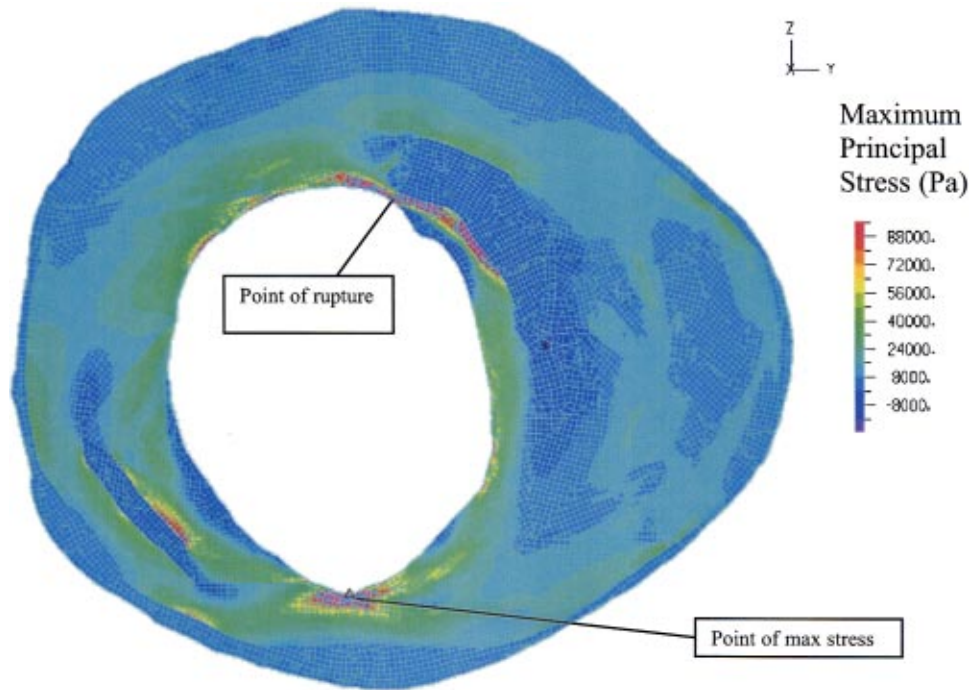


Fig. 5 Maximum principal stress band plot (Pa) for a transversely isotropic trial of average parameters. The triangle indicates the point of maximum stress while the star indicates the point of minimum stress. In the transversely isotropic and nonlinear isotropic with residual strain runs, the point of maximum stress is in an area of artificial stress concentration.

(average) values of each parameter for each material. Analyses were then conducted in which one of the four defining parameters of each orthotropic material (Table 1), or one of the two defining parameters of each isotropic nonlinear material (Table 2), was varied by $\pm 10\%$, $\pm 20\%$, and $\pm 50\%$. An exception was made for the Young's modulus of lipid, which was varied over its known range (35% to 260% of its initial value) only for the anisotropic trials [8].

It is important to note that because some parameters were specified in relation to others as described above, when one was varied, the other related parameters were altered as well. This is because the nonlinear material parameters are based on two values, a/b and $b/2$ [see Eq. (1)]. When a is varied, only the first parameter changes. However when b is varied, both parameters change.

Results and Discussion

Mean Stress and Strain Levels. Stress distributions for the three types of analysis, namely isotropic nonlinear (with and without residual strains) and anisotropic linear, are shown in Figs. 4(a), (b), and 5, respectively. Whereas the distributions are generally similar, there are several differences of note. The maximum level of stress in the nonlinear case (without residual strains) is located at the site of rupture, while the anisotropic and nonlinear

Table 3 Maximum principal stress and strain values at baseline parameters for Isotropic and Anisotropic cases.

	Isotropic Nonlinear w/Residual Strain		Isotropic Nonlinear		Anisotropic Linear	
	Stress (kPa)	Strain	Stress(kPa)	Strain	Stress (kPa)	Strain
RUP	314.532	0.097	399.91	0.099	552.334	0.196
TP1	49.088	0.018	49.799	0.017	77.345	0.032
TP2	12.229	0.007	12.153	0.005	9.942	0.003

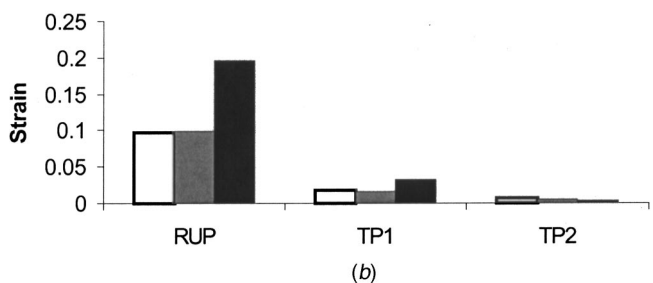
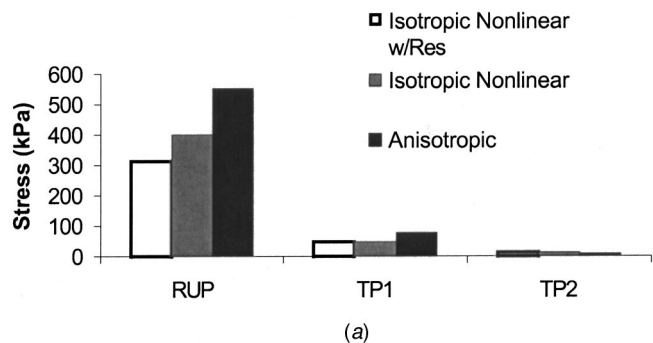


Fig. 6 Graphical representation of maximum principal stress (panel a) and strain (panel b) vs. location in specimen for anisotropic and isotropic nonlinear (with and without residual strains). The specific locations in the specimen were: RUP, the rupture site, TP1, test point one, and TP2, test point two (see Fig. 2). The region (artery, fibrous, etc.) identifies in which portion of the model the parameters were changed in a given test (color coded in Fig. 2). Legend in (a) is applicable to both panels.

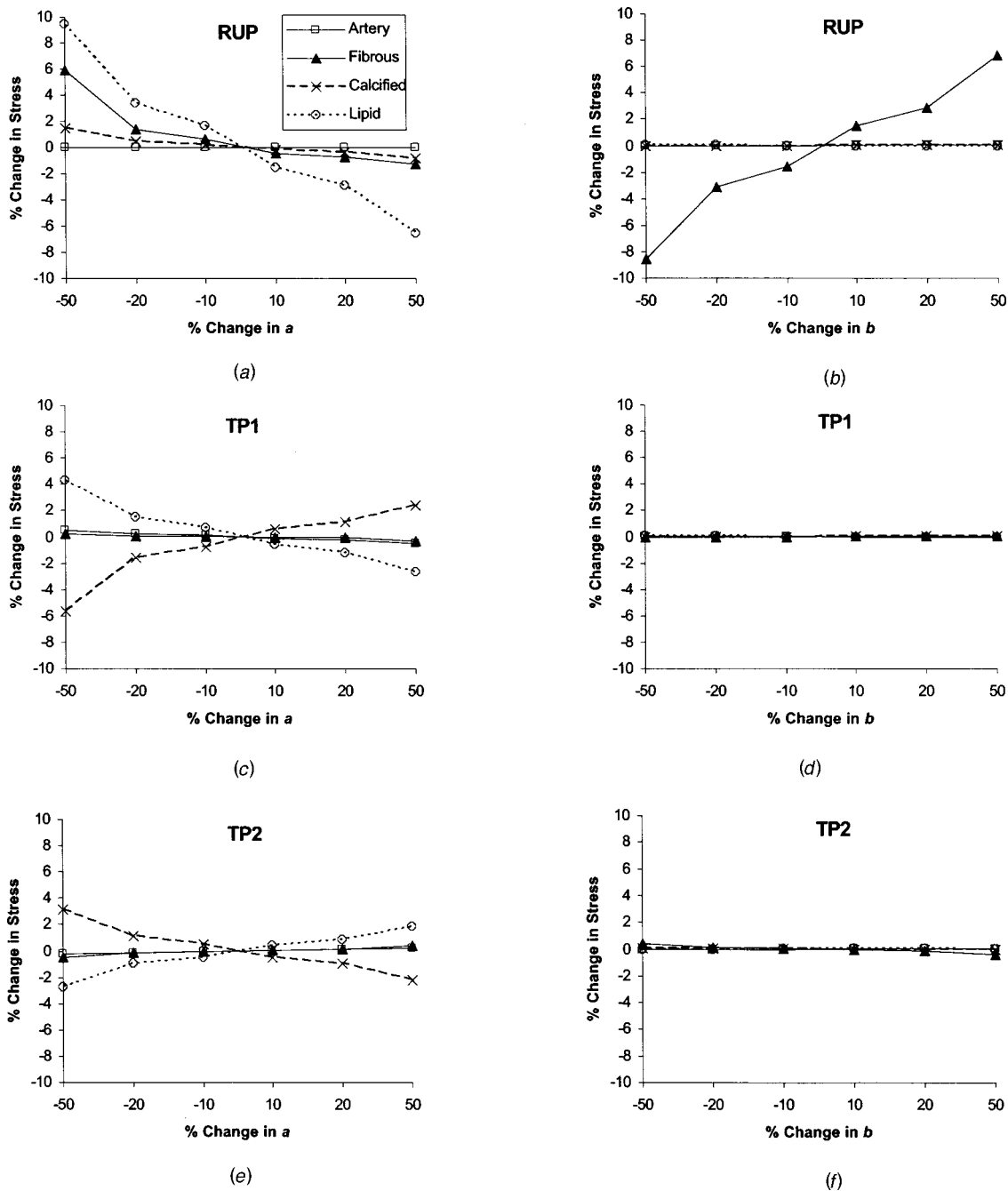


Fig. 7 Sensitivity of maximum principal stress (in % change from nominal values) for the isotropic nonlinear without residual strains model, vs. % change in a (left panel) and b (right panel) coefficients of the corresponding material as indicated in legend of (a). Legend in (a) is applicable to all plots.

with residual strains models predict peak stress at a remote site where the vessel wall seems to exhibit a sharp corner (see Figs. 4(a), (b) and 5 to locate the site of peak stress). This is presumably artificial but illustrates an important potential source of error in this type of calculation.

The maximum principal stress levels when all parameters are fixed at their calculated values serve as the baseline conditions for the sensitivity analysis. These values are provided in Table 3 [Figs. 6(a)–(f)].

The isotropic (anisotropic) level of stress at the rupture site is approximately 1.5 times (2 times) that previously used as a threshold value for plaque rupture [1]. Although values at the three sites

are generally consistent, stress at the site of rupture is somewhat reduced by the addition of residual strain, and increased by introducing the linear orthotropy of the specimen.

Isotropic Nonlinear Analysis. Sensitivity results in the form of the percentage change in stress or strain are presented in Figs. 7–9, for the isotropic nonlinear analyses with and without residual strain, respectively. As can be seen, when the modulus, or a , the nonlinear material analog, is varied, changes in stress are relatively small for a $\pm 10\%$, $\pm 20\%$, and $\pm 50\%$ variation. Specifically, a 50% change in a and b yields less than a 10% change in the maximum stress. The changes in strain, however, are compa-

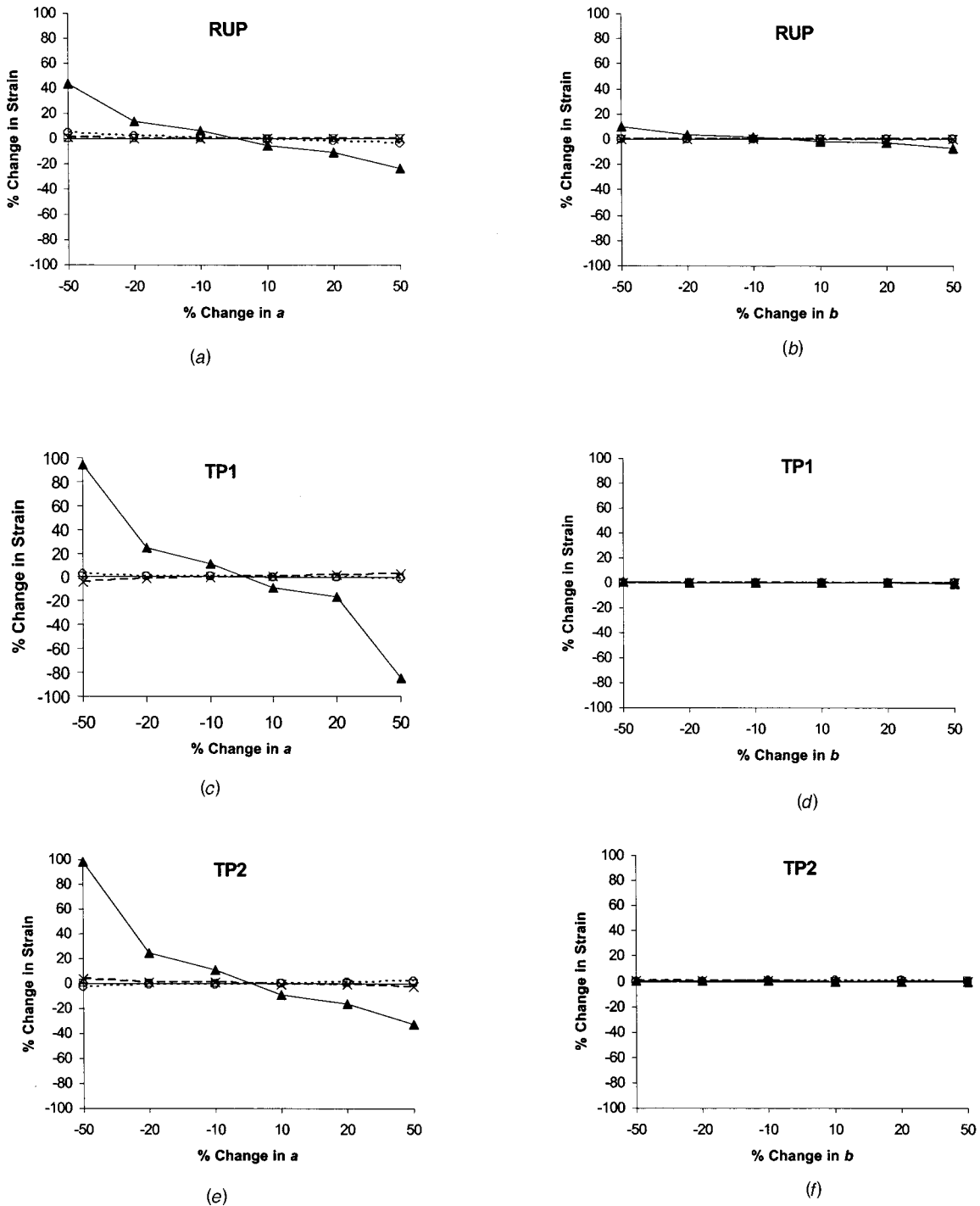


Fig. 8 Sensitivity of maximum principal strain (in % change from nominal values) for the isotropic nonlinear model without residual strains, vs. % change in *a* (left panel) and *b* (right panel) coefficients of the corresponding material as indicated in legend of (a). Legend in (a) is applicable to all plots.

rable to the variation in *a*, which is more pronounced in the fibrous plaque data since all three points lie in fibrous plaque. This reflects the fact that the stresses must balance the average loads. Thus changes in stress can only result from changes in the distribution of stress across the wall, and these are apparently small. Strain, however, must directly reflect any change in modulus.

Effects due to changes in arterial wall properties are particularly small since the points of interest lie within fibrous plaque and the arterial wall contributes little in supporting the overall load. The effects of varying *b* in the nonlinear model were generally very

small throughout all materials, except fibrous plaque which exhibited a significant, yet less than 10%, change in stress when *b* was varied by as much as 50%.

Examining the plots of the sensitivity analysis in Figs. 7 and 8, some general trends are visible across the variations in *a* and *b* for all four of the materials. The general trends in all of the plots shows that as *a* and *b* increase, the stress and strain decrease at the rupture point. Most noticeable is the change in stress and strain at the rupture point due to variation of fibrous plaque and lipid parameters. This is consistent with the fact that the rupture

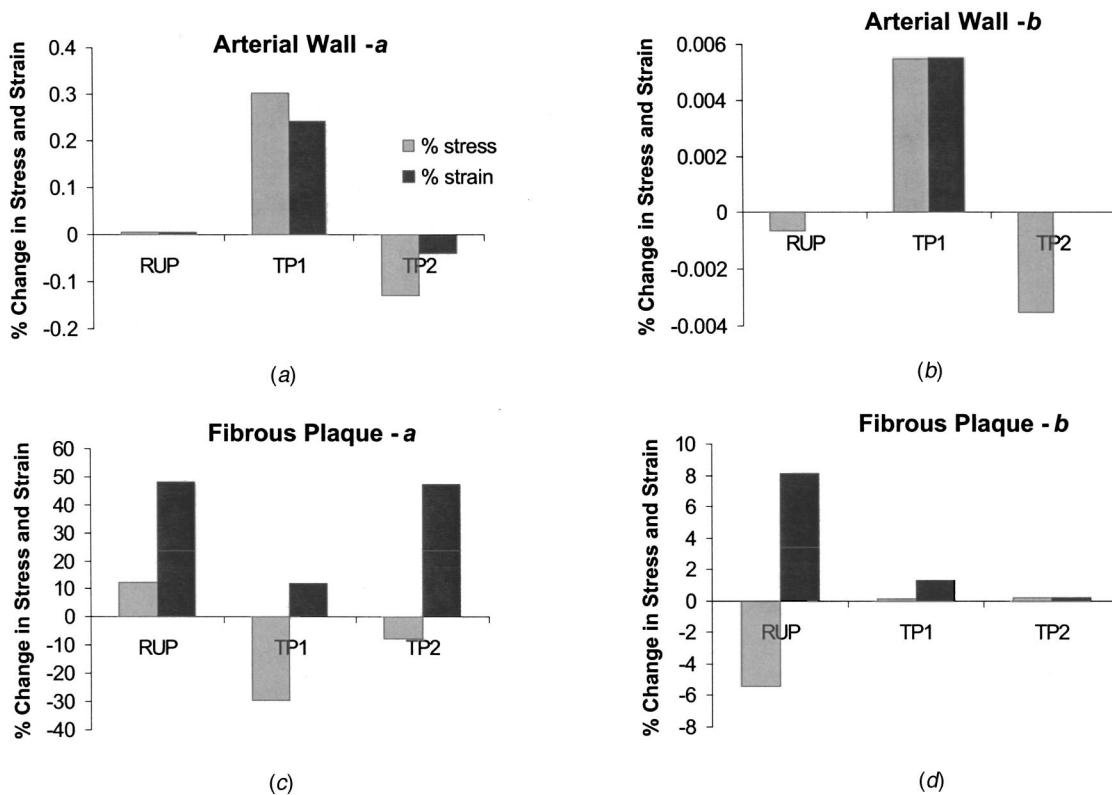


Fig. 9 Sensitivity of maximum principal stress and strain for the isotropic model with nonlinear residual strains, due to a -50% change in a (left panel) and b (right panel) of the corresponding material as indicated in each panel.

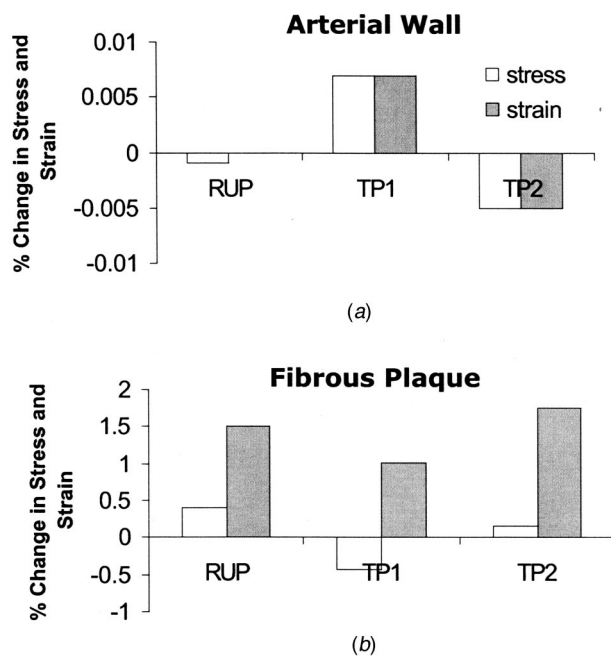


Fig. 10 Sensitivity of maximum principal stress and strain for the anisotropic model, due to -10% change in ν_{0z} of the corresponding material as indicated in each panel.

point (RUP) resides in the fibrous cap shoulder and near the lipid pool. While all three points (RUP, TP1, and TP2), show significant sensitivity to fibrous plaque parameters (all three lie in fibrous plaque regions), TP1 shows sensitivity to other materials as well. TP1 is located near a lipid pool and an area of calcification so it will be more likely to exhibit stress change due to variation in the parameters of lipid and calcified plaque. The strain at TP1 is less affected by lipid and calcification and primarily governed by fibrous plaque properties.

The general trend of decreasing stress and strain with increasing a , may be explained from the nature of a . Since a is effectively the nonlinear counterpart of the elastic modulus, any increase in a reflects the stiffening of the material. Although qualitatively similar trends are shown by sensitivity of strain to a and b , variation in b yields a much (two orders of magnitude) smaller change in strain variation (see Fig. 8). This can be explained from the present formulation of strain energy density function, as the exponential term compensates for the prefactor denominator.

Results for the nonlinear analysis with residual strain are presented in Fig. 9. Considering the striking similarity observed (see Fig. 6) between stress and strain for the nonlinear trials with and without residual strain, only a few trials were run for this model to prove that the nonlinear model with residual strains has the same sensitivity as the nonlinear model without them (see Fig. 9).

Anisotropic Analyses. The anisotropic trials (Fig. 10) are generally consistent with the isotropic ones. For both cases, the variation of stress is similar across material parameters and test points. Also, the normal arterial wall material properties have little effect on maximum principal stress or strain, and the variation of ν for the lipid trials exhibits a tendency for greater deviation as ν approaches the incompressible limit of 0.5.

For the anisotropic trials, the sensitivity between positive and

negative variations were symmetric throughout with the exception of the change in ν for calcified and lipid materials.

While we are confident of the broad conclusions reached in this study, it is important to recognize several limitations. Clearly, the real diseased artery is a complex three-dimensional structure that can only be captured in an approximate sense with a two-dimensional model. Also, the partitioning of the wall into four uniform zones is obviously a gross simplification. It will be some time before we can more accurately portray the true geometry, structure, and composition, however, and this remains an active area of investigation.

Conclusion

Based on these results, the currently known parameters of the arterial wall, fibrous plaque, calcified plaque, and lipid pool parts of plaque have low sensitivities for a $\pm 10\%$, $\pm 20\%$, $\pm 50\%$ variation in the nonlinear material properties, as well as a $\pm 10\%$ variation in orthotropic material properties. This insensitivity to variations in a and b is true for both isotropic nonlinear models, with and without residual strains. Therefore, stress analysis may be used with confidence that the material properties contribute relatively small errors, recognizing, however, that the magnitude of uncertainty in strain is of the same order as uncertainties in elastic modulus of the fibrous plaque region. Images need to be closely scrutinized, however, to ensure that artifactual stress concentrations do not arise due to unrealistically sharp corners. Either isotropic or anisotropic models provide useful estimates, however the predictions in regions of stress concentration (e.g., the site of rupture) are somewhat more sensitive to the specific model used, increasing by up to 30% from the isotropic nonlinear to orthotropic linear model in the present example, however not changing significantly when residual strains are included in the isotropic nonlinear model.

Acknowledgments

The specimen for this study was provided by Renu Virmani of the Armed Forces Institute of Pathology, Department of Cardio-

vascular Pathology, Washington, DC. The authors would also like to thank Dr. Richard Lee of the Brigham and Women's Hospital, Cardiovascular Division, Boston, MA for his contributions to the present study. Support from the National Heart, Lung, and Blood Institute (HL061794) is gratefully acknowledged.

References

- [1] Cheng, G. C., Loree, H. M., Kamm, R. D., Fishbein, M. C., and Lee, R. T., 1993, "Distribution of Circumferential Stress in Ruptured and Stable Atherosclerotic Lesions," *Circulation*, pp. 1179–1187.
- [2] Richardson, P. D., Davies, M. J., and Born, G. V. R., 1989, "Influence of Plaque Configuration and Stress Distribution on Fissuring of Coronary Atherosclerotic Plaques," *Lancet*, pp. 941–944.
- [3] Humphrey, J. D., 1995, "Mechanics of the Arterial Wall: Review and Directions," *Crit. Rev. Biomed. Eng.*, **23**, pp. 82–90.
- [4] Loree, H. M., Grodzinsky, A. J., Park, S. Y., Gibson, L. J., and Lee, R. T., 1994, "Static Circumferential Tangential Modulus of Human Atherosclerotic Tissue," *J. Biomech.*, **27**, pp. 195–204.
- [5] Patel, D. J., Janicki, J. S., and Carew, T. E., 1969, "Static Anisotropic Elastic Properties of the Aorta in Living Dogs," *Circ. Res.*, **25**, pp. 765–779.
- [6] Jones, R. M., 1975, "Macromechanical Behavior of a Lamina," in *Mechanics of Composite Materials*, New York, McGraw-Hill Book Co., pp. 31–47.
- [7] Loree, H. M., Kamm, R. D., Stringfellow, R. G., and Lee, R. T., 1992, "Effects of Fibrous Cap Thickness on Peak Circumferential Stress in Model Atherosclerotic Vessels," *Circ. Res.*, **71**, pp. 850–858.
- [8] Loree, H. M., Tobias, B. J., Gibson, L. J., Kamm, R. D., Small, D. M., and Lee, R. T., 1994, "Mechanical Properties of Model Atherosclerotic Lesion Lipid Pools," *Arterioscler. Thromb.*, **14**, pp. 230–234.
- [9] Bathe, K. J.: *Finite Element Procedures*. Saddle River, New Jersey, Prentice Hall, Inc, 1996, p 290.
- [10] Delfino, A., Stergiopoulos, N., Moore, Jr., J. E. and Meister, J. J., 1997, "Residual Strain Effects on the Stress Field in a Thick Wall Finite Element Model of the Human Carotid Bifurcation," *J. Biomech.*, **30**, pp. 777–86.
- [11] Holzapfel, G. A., Gasser, T. C., and Ogden, R. W., 2000, "A New Constitutive Framework for Arterial Wall Mechanics and a Comparative Study of Material Models," *J. Elast.*, **61**, pp. 1–48.
- [12] ADINA: Automatic Dynamic Incremental Nonlinear Analysis, Watertown, MA.
- [13] Dobrin, P. B., 1986, "Biaxial Anisotropy of Dog Carotid Artery: Estimation of Circumferential Elastic Modulus," *J. Biomech.*, **19**, pp. 351–358.